Rayleigh-Taylor instability under a shear stress free top boundary condition and its relevance to removal of mantle lithosphere from beneath the Sierra Nevada

Christopher Harig,[1] Peter Molnar,[1] and Gregory A. Houseman[2]

Received 29 November 2007; revised 19 September 2008; accepted 31 October 2008; published 31 December 2008.

[1] The separation of zones of apparent downwelling flow at the ends of the Sierra Nevada suggests a relatively large wavelength (~500 km) of unstable growth, but Rayleigh-Taylor instabilities for plausible rheological structures with a fixed top boundary condition require much shorter wavelengths (<100 km) for maximum growth rates. To understand this difference, we analyze analytical solutions and perform numerical 2-D plane strain experiments for Rayleigh-Taylor instability of a dense layer overlying a less dense substratum, representing the instability between the mantle lithosphere and the underlying asthenosphere, focusing on the effects of a shear stress free boundary condition at the top. The overall effect of this condition is an enhancement of growth rate factors at long wavelengths, which depends greatly on the exponential viscosity variation with depth of the layer. With large or little variation across the unstable layer, the solutions approximate those with a fixed top boundary condition or for constant viscosity, respectively. An intermediate zone showing the enhanced growth rates includes ratios of layer thickness to viscosity e-folding length, *h/L*, of ~1–8 for Newtonian viscosity and ~1–4 for nonlinear viscosity. The free top condition is likely applicable to geologic situations where the lower crust is weak. Olivine flow laws and low-temperature estimates at 35 km depth (255–355°C) place the Sierra Nevada viscosity scaling ratio, *h/L*, between 5 and 9. Thus longer wavelengths than commonly assumed for Rayleigh-Taylor instabilities seem permissible when viscosity decreases with depth and the top surface of the layer is only weakly constrained. **Citation:** Harig, C., P. Molnar, and G. A. Houseman (2008), Rayleigh-Taylor instability under a shear stress free top boundary condition and its relevance to removal of mantle lithosphere from beneath the Sierra Nevada, *Tectonics*, *27*, TC6019, doi:10.1029/2007TC002241.

[1]Department of Geological Sciences, Cooperative Institute for Research in Environmental Science, University of Colorado, Boulder, Colorado, USA.

[2]Institute of Geophysics and Tectonics, School of Earth and Environment, University of Leeds, Leeds, UK.

0278-7407/08/2007TC002241$12.00

1. Introduction

[2] The conductive temperature profile across the mantle lithosphere indicates that the mantle lithosphere should be more dense than the underlying upper mantle when brought to the same pressure, assuming no compositional differences. This density contrast is inherently unstable. Small temperature, and hence density, perturbations to this layering are normally destroyed by thermal diffusion, but if a perturbation is large or can grow fast enough, thermal diffusion can be neglected owing to its long time scale. In this case, the mantle lithosphere can be treated as a case of Rayleigh-Taylor instability [*Canright and Morris*, 1993; *Chandrasekhar*, 1961; *Conrad and Molnar*, 1997]. For Newtonian viscosity, density perturbations will initially grow exponentially with time. When perturbations grow to several tens of percent of the unstable layer thickness, sinking regions will downwell into the upper mantle super-exponentially [e.g., *Canright and Morris*, 1993]. As it is removed, mantle lithosphere will be replaced with less dense asthenosphere in the isostatic column. Therefore this removal would cause the surface to rise to maintain pressure balance [e.g., *Bird*, 1978; *England and Houseman*, 1989].

[3] In Tibet, an area of much current study, convective removal of thickened Asian lithosphere is one [*Houseman et al.*, 1981] of many tectonic processes proposed to occur beneath the Tibetan Plateau in response to the Indian-Eurasian collision [e.g., *Dewey and Bird*, 1970; *Dewey and Burke*, 1973; *Ni and Barazangi*, 1983; *Owens and Zandt*, 1997; *Willett and Beaumont*, 1994; *Zhao and Morgan*, 1985]. The upper mantle of the Tibetan Plateau is characterized by large east–west seismic wave speed gradients and attenuation, and possible north–south wave speed gradients [e.g., *Dricker and Roecker*, 2002; *McNamara et al.*, 1997; *Molnar*, 1990; *Ni and Barazangi*, 1983; *Woodward and Molnar*, 1995]. Additionally, tomographic imaging has revealed what seems to be a narrow zone of downwelling mantle lithosphere beneath central Tibet [*Tilmann et al.*, 2003]. Together, these observations suggest a dynamic origin for some of the plateau's deformation such as high mean elevation and the distribution of normal faulting across the plateau [*Houseman and Molnar*, 1997]. What remains uncertain, however, is the length scale of mantle lithosphere deformation. Studies covering both large areas, such as that by *Dricker and Roecker* [2002] (~25°), and small areas, such as that by *Tilmann et al.* [2003] (~5°), show lateral variations in the upper mantle on these scales.

[4] In the Sierra Nevada in California, the evidence favoring removal of mantle lithosphere from beneath the

range is clearer. Examination of entrained xenoliths between depths of 40 and 100km from before 8 Ma indicate the presence of a 40–60 km eclogite-rich layer beneath the Sierran batholith in the crust [*Ducea and Saleeby*, 1996, 1998; *Lee et al.*, 2001]. Magmatism at 3.5 Ma and additional xenoliths erupted since imply the absence of this eclogite layer and presumably its removal by this time, and logically, the deeper mantle lithosphere as well [*Farmer et al.*, 2002]. Indications of this removal event are also seen in geomorphic observations. For instance, there is evidence of tilting with an increase in height of the range crest on its western range flank [e.g., *Stock et al.*, 2004; *Unruh*, 1991], a fairly uniform westward shift of the edge of normal faulting and horizontal extension around 3.5 Ma, and possible initiation of folding and thrust faulting along the western margin of the Sierran microplate [*Jones et al.*, 2004].

[5] Two high seismic wave speed anomalies, the Isabella and Redding anomalies, extending to more than 250 km depth beneath the Central Valley near the ends of the range are likely locations for the removed lower lithosphere (Figure 1) [*Benz and Zandt*, 1993; *Jones et al.*, 1994; *Reeg et al.*, 2007]. Both the Isabella [*Jones and Phinney*, 1999] and the Redding anomalies [*Hartog and Schwartz*, 2000; *Özalaybey and Savage*, 1995] are seismically isotropic which can be characteristic of eclogites [*Fountain and Christensen*, 1989]. Furthermore, the area above the Isabella anomaly is undergoing active subsidence, which would be expected over such a downwelling [*Saleeby and Foster*, 2004]. Certainly, there is not complete north–south symmetry to the Sierra Nevada Pliocene history, as the passing of the southern edge of the Gorda plate and Mendocino Fracture Zone illustrates [*Atwater and Stock*, 1998]. But, it seems more likely than not that the two anomalies are the result of the same process, and very reasonable to postulate so [*Jones et al.*, 2004; *Le Pourhiet et al.*, 2006].

[6] Although Rayleigh-Taylor experiments have been carried out for no-slip top boundary conditions and differing rheological structures, the ≈500 km separation of the Sierran anomalies is significantly longer than the wavelength for the peak growth rates for these conditions. Simple experiments (constant viscosity, constant density) have shown that the wavelength corresponding to maximum growth rate factor is about three times the unstable layer thickness ($\lambda_{max} \approx 3h$) [e.g., *Conrad and Molnar*, 1997]. Other experiments have shown that a buoyant crustal layer also influences the growth rate of instabilities and suppresses growth of longer wavelengths [*Neil and Houseman*, 1999]. We explore what other factors might influence the Rayleigh-Taylor instability process to favor the growth of longer wavelength perturbations and downwellings.

[7] Our goal is to determine the effects of a shear stress free boundary between the crust and mantle lithosphere on growth rates of Rayleigh-Taylor instability under various rheological stratification, such as exponentially varying viscosity with depth. This boundary condition represents one possible end member, with the other being a no-slip top boundary condition. The state of Sierran lithosphere at the time convective removal began was surely in between these two idealized states. Arguments can be made, however, that both are reasonable approximations.

[8] The thermal structure of the lithosphere around 10 Ma can be inferred from several measures. The present-day surface heat flux in the western Sierra is very low (18–60 mW m^{-2}), and can bound the temperature at 35 km depth to 255–355°C simply by assuming a steady state [*Lachenbruch and Sass*, 1977; *Saltus and Lachenbruch*, 1991]. Separate temperature estimates from xenolith geothermometry can bound the temperature at greater depth, 130 km, to only 925°C [*Ducea and Saleeby*, 1998]. A steady state using this measurement would indicate a temperature at 35 km depth of similar range to before, 250–350°C [*Molnar and Jones*, 2004]. Thus, on the one hand, very low lithosphere temperatures might be used to assume a no-slip condition at the Moho with an undeforming crust. Alternatively, as mentioned, the Sierra Nevada is estimated to have had a 40–60 km thick eclogite-rich layer beneath the batholith [*Ducea and Saleeby*, 1996, 1998; *Lee et al.*, 2001]. Field observations of eclogite and granulite [e.g., *Austrheim*, 1991] have shown that eclogites can deform with much lower viscosity than their granulite protoliths. Moreover, the felsic quartz-rich upper crust that survives today could have been weak even at the low temperatures estimated for depths of 30–40 km, for quartz flows at relatively low shear stress at such temperatures [e.g., *Brace and Kohlstedt*, 1980; *Sibson*, 1977, 1982].

[9] *Jull and Keleman* [2001] examined the conditions under which dense mafic lower crustal material could become convectively unstable. Under their most extreme circumstances, such as an assumed background strain rate of 10^{-14} s^{-1}, Moho temperatures as cold as 550–650°C could produce an instability in 10 Ma for a dense layer 10 km thick immediately below. Given estimates for a Sierran eclogite layer are much thicker, it is possible the bottom several kilometers were at or above this range of temperatures. An instability initiated in the Sierra mantle lithosphere could provide the background strain rate necessary, and eclogite could be swept along with lower material. Thus, if viscosity of the middle crust were sufficiently low, the top boundary condition appropriate for removal of this eclogite layer with the underlying mantle lithosphere could be approximated by a shear stress free boundary, either at the Moho or within the eclogite layer. Here, we present both analytical and numerical solutions to idealized problems with this stress free boundary above our unstable layer.

2. Background Theory and Methods

[10] The Rayleigh-Taylor instability problem in the Earth is one of Stokes flow for viscous fluids, representing a balance between body forces and surface tractions after assuming incompressibility and neglecting inertial terms. The governing equation takes the form:

$$\frac{\partial \sigma_{ij}}{\partial x_j} - \rho g \delta_{iz} = 0 \tag{1}$$

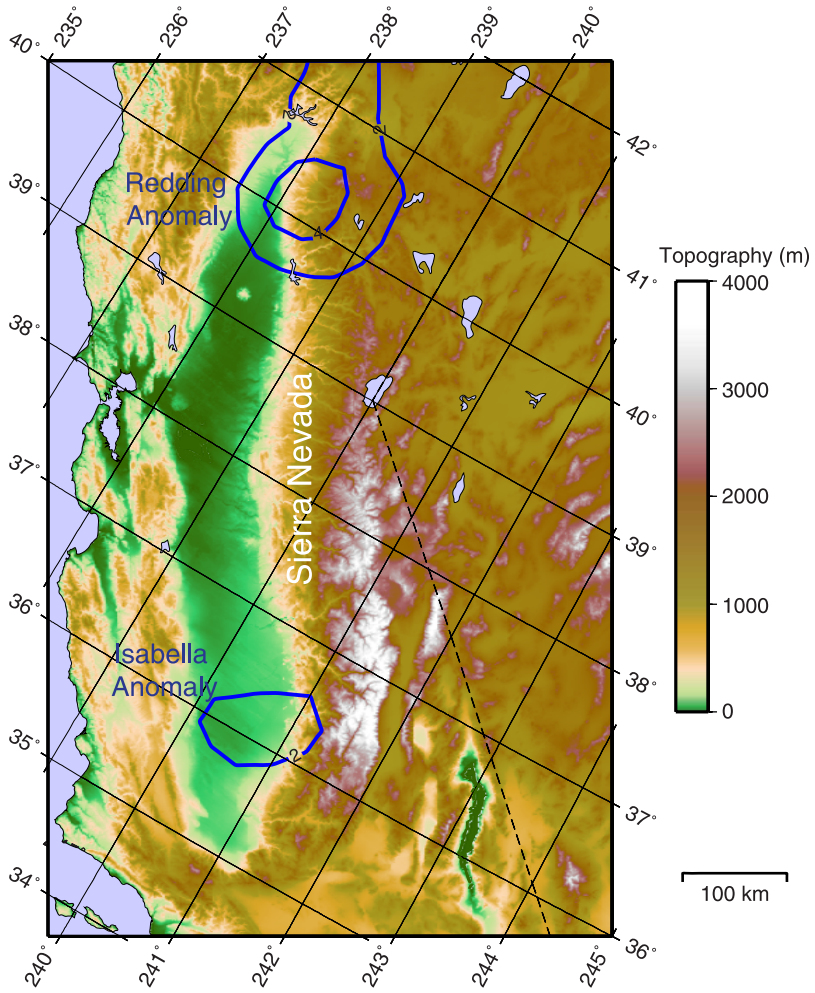

Figure 1. Map view of the Sierra Nevada range in California with colored topography from the Global Land One-km Base Elevation (GLOBE) Project. High-speed seismic anomalies at about 150 km depth are contoured in percent V_p perturbation from the IASP91 model. Tomography contour provided from *Reeg et al.* [2007].

where σ_{ij} are stress components, x_j are spatial coordinates, ρ is density, g is gravity, and δ_{ij} is the Kronecker delta. We solve equation (1) for a material layer overlying a less dense half-space (or a subspace of finite depth) seen schematically in Figures 2 and 3. We allow for a general nonlinear constitutive equation between deviatoric stress, τ_{ij}, and strain rate, $\dot{\epsilon}_{ij}$,

$$\tau_{ij} = B\dot{E}^{(1/n-1)}\dot{\epsilon}_{ij} \tag{2}$$

where $\dot{E}$ is the second invariant of the strain rate tensor, n is the rheological exponent, and B is the viscosity coefficient. Under familiar Newtonian rheology, $n = 1$, and we have the relation $\eta = (1/2)B$. For a non-Newtonian fluid, $n > 1$, viscosity is strain-rate-dependent as $\eta_{eff} = (1/2)B\dot{E}^{(1/n-1)}$, where η_{eff} is an effective viscosity, which changes as strain rates change with time.

[11] Temperature gradients inherent to the mantle lithosphere will cause viscosity to vary within the layer. Laboratory experiments have shown that linear temperature gradients translate approximately to an exponential variation of viscosity with depth [e.g., *Fletcher and Hallet*, 1983]. We therefore consider cases in which B varies exponentially with depth, as seen in Figure 2. Depth, z, is set to zero at the interface between layers of different density and decreases downward. Viscosity, η, then takes the form:

$$\bar{\eta} = \eta_0 e^{(\gamma z)} \tag{3}$$

where η_0 is the viscosity at the layer interface, and $1/\gamma = L$ is the viscosity (e-folding) decay length. Various values of decay length are used so that over a layer of thickness h we have $h\gamma = 1, 2, 4$, etc.

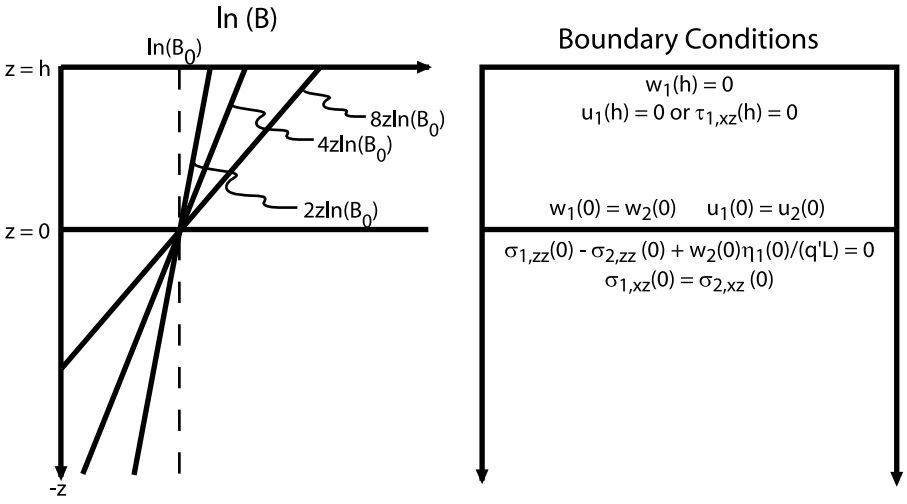

Figure 2. (left) Viscosity structure and (right) linear stability boundary conditions. Depth, z, is zero at the bottom interface of the unstable layer and decreases downward; $z = 0$ represents the bottom of the mantle lithosphere, and $z = h$ represents the shear stress free top surface, which could be either at the Moho or within the lower crust. We include the unused fixed-top condition to better show the difference to previous work. Viscosity is an exponential function with depth, and B is the viscosity coefficient. Subscripts of 1 are for quantities in the layer, while subscripts of 2 are quantities of the lower half-space.

[12] We also perform calculations with different density structures. The majority of our work is done with a constant density difference. For a few cases we use density decreasing linearly with depth in the layer, as would be the case for a linear temperature gradient in the lithosphere and a constant coefficient of thermal expansion. Linear density takes the form

$$\rho(z) = \frac{2\Delta\rho}{h} z \tag{4}$$

so that over a layer of thickness h, the dimensionless $(\rho(z)/\Delta\rho)$ density at the top and bottom surfaces are 2 and 0 respectively, and we have the same total mass anomaly in the layer in both sets of experiments. The density anomaly in the substrate is zero.

[13] To simplify solutions, we nondimensionalize growth rate factors (q) and wave numbers (k) by the appropriate length and time scales. Symbols used here and elsewhere are listed in the notation section. For exponentially varying Newtonian viscosity with depth we have

$$q'_L = q\frac{2\eta_0}{\Delta\rho g L}, \qquad k'_L = kL \tag{5}$$

with subscripts denoting the choice of nondimensionalization as in the work by *Molnar et al.* [1998]. The time scale $2\eta_0/\Delta\rho g L$ is determined from the time required to produce unit strain under a deviatoric stress of magnitude $\Delta\rho g L$. We also devote some discussion later to comparisons between cases with large viscosity variations and those with no viscosity variations, given the different nondimensionalizations required.

[14] We perform linear stability analyses for cases with constant density to find analytical solutions for growth rate factor, q' as a function of dimensionless wave number,

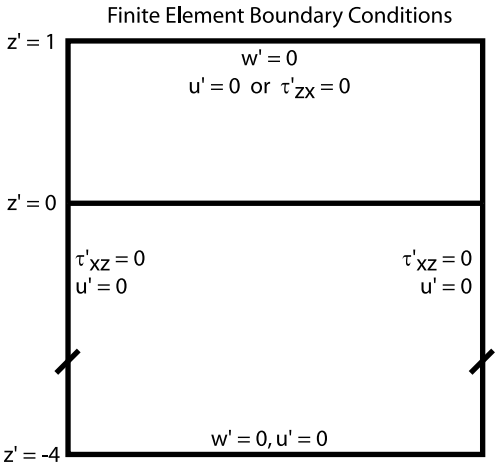

Figure 3. Finite element calculation boundary conditions for a viscous half-space. Again, $z' = 0$ is the bottom of the unstable layer (i.e., the mantle lithosphere), and $z' = 1$ represents the shear free top surface (i.e., at the Moho or within the lower crust). We also include the unused fixed-top condition to better show the difference to previous work. In calculations with an inviscid half-space, the mesh extends from 0 to 1.

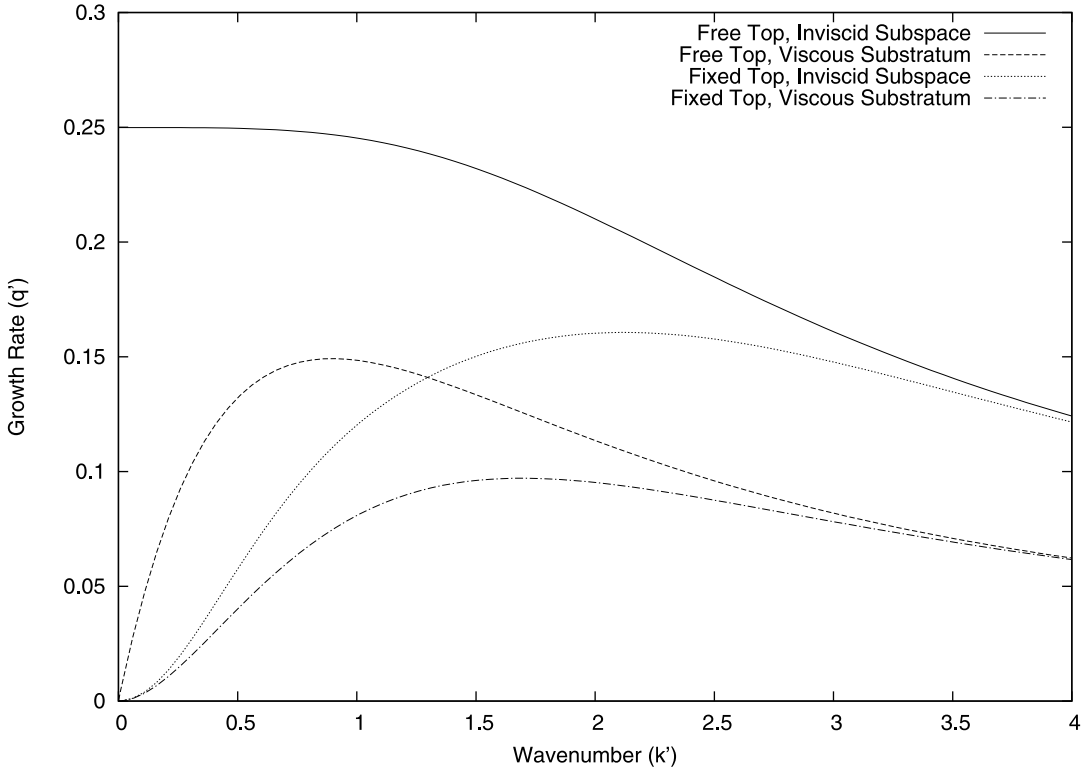

Figure 4. Linear stability analysis curves of growth rate factors (q') versus wave number (k') for simple, previously known experiments. The free-top cases were discussed briefly by *Hoogenboom and Houseman* [2006], and substratum viscosity was explored by *Molnar et al.* [1998], though with a fixed-top condition. These cases have density and viscosity constant with depth but that vary in their top boundary condition and subspace viscosity.

$k' = kL$. With linear stability, the assumed form of solution for $n = 1$ cases is

$$W(z)f(x,y)e^{qt} \tag{6}$$

where

$$\nabla^2 f(x,y) = -k^2 f(x,y). \tag{7}$$

$W(z)$ is the function of downward velocity dependent on z and $f(x, y)$ is a harmonic function with wave number k, here assumed to be $\cos(kx)$. We consider only first-order perturbations to background stress and strain rates, and follow the approach of *Conrad and Molnar* [1997]. The boundary conditions for these cases are shown in Figure 2.

[15] Linear stability analyses are paired with 2-D plane strain numerical calculations using the finite element program Basil (http://homepages.see.leeds.ac.uk/~1eargah/basil/). For numerical experiments of a layer over an inviscid half-space, a single layer of triangular mesh is created from $0 \leq z \leq h$ and a harmonic perturbation of $0.01(1-z)$ amplitude is applied to the mesh. Velocity fields and subsequent deformation are then calculated iteratively through time. For cases of a viscous substratum, we follow a similar process, but the mesh is extended from $-4h \leq z \leq 1h$. This depth is chosen to strike a balance between minimizing the influence of the bottom boundary of the substratum and the calculation requirements of a finer mesh. Boundary conditions for the calculation are shown in Figure 3. For each experiment the bottom boundary of the unstable layer is perturbed using a specific wavelength equal to twice the width of the box, and to sample the k' spectrum we varied the horizontal dimension of the box. For Newtonian viscosity calculations, $n = 1$, we fit $|Z'|$, the absolute value of the vertical coordinate of the maximum downwelling, versus dimensionless time, t' ($= \Delta\rho g L/2\eta_0$), to a straight line of the form

$$\ln|Z'| = \ln Z_0 + q'_{est}t' \tag{8}$$

to estimate the growth rate factor, q'_{est}. Line fitting is limited to the section of growth that follows the decay of initial transient, and before growth to large amplitudes (a few tens of percent). We plot both growth rate curves from linear stability analyses and numerical values of q'. In general the numerical results agree within 3% of linear stability analyses.

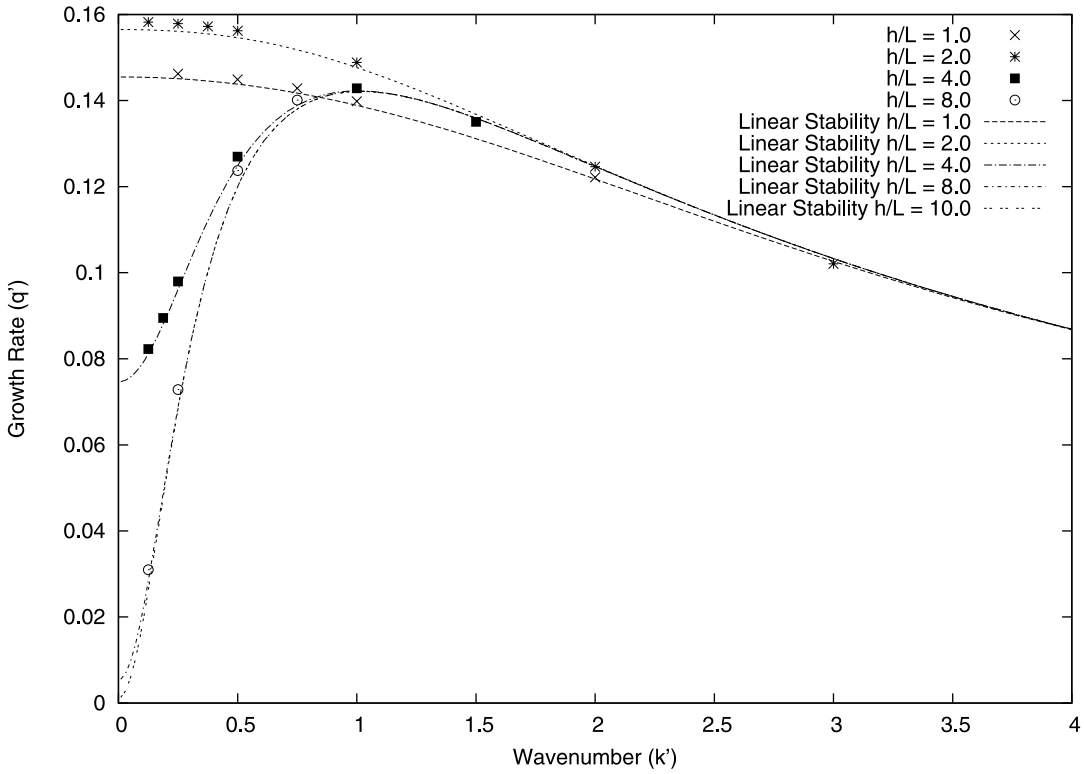

Figure 5. Growth rate versus wave number for various values of h/L. Dashed lines are results of linear stability analysis. Points are results of numerical calculations. This experiment is a layer over an inviscid half-space. The layer has exponentially varying viscosity and a stress free top boundary condition. Note that curves for linear stability $h/L = 8$ and 10 are coincident everywhere except close to $k' = 0$.

[16] For calculations with a nonlinear (non-Newtonian) viscosity relation we use a power law exponent of $n = 3$. Following *Houseman and Molnar* [1997], lines of the form

$$Z'^{(1-n)} = (n-1)\left(\frac{C}{n}\right)^n \left(t'_b - t'\right) \tag{9}$$

with $t' = t(\Delta\rho g L/B)^n$ are fit to the output position data Z'. Here, t'_b represents the time when the downward speed of the downwelling approaches infinity, signaling when the blob would drop off completely from the layer. C is a dimensionless parameter analogous to the growth rate factor, q', in Newtonian calculations, which we will use to compare growth rates for various wave numbers.

3. Exponentially Varying Newtonian Viscosity With Depth

3.1. Inviscid Substratum and Constant Density

[17] In the most basic Rayleigh-Taylor experiments there is a fundamental difference between using a no-slip and a free-slip boundary condition at the top of the unstable layer. The use of a no-slip boundary condition ensures that as k' approaches zero, the growth rate factor q' also approaches zero [e.g., *Conrad and Molnar*, 1997; *Molnar et al.*, 1998; *Whitehead and Luther*, 1975]. When the free-slip condition is used, however, q' can be finite in the limit of small k', as in the linear stability analysis in Figure 4. We plot four simple cases with constant viscosity and density to illustrate this difference, and show how the addition of a viscous substratum can retard growth. Here, the case with a free top and an inviscid subspace maintains a finite value near $k' = 0$, but the other cases trend to 0 when $k' \rightarrow 0$. We further examine this difference with more complex, depth-varying physical properties.

[18] If there is significant viscosity contrast between the mantle lithosphere and asthenosphere, any motion will be dominated by the viscosity of the lithosphere. In this instance, the asthenosphere can be approximated by an inviscid substratum of infinite depth by setting the ratio $\eta_{astheno}/\eta_{man.\ lith} \rightarrow 0$. Considering this assumption in the context of stagnant lid convection, we can imagine how the mantle lithosphere could deform irrespective of asthenosphere influence [*Moresi and Solomatov*, 1995]. We begin by examining cases that use this approximation for the subspace and depth varying viscosity in the unstable layer above it. We examined a range of h/L values with results shown in Figure 5. These calculations exhibit two styles of growth. For large viscosity variations across the layer ($h/L >$ 8), growth rate curves approach those for the case with exponential viscosity in two infinite half-spaces, from *Conrad and Molnar* [1997]. The viscosity in the top part of the layer becomes so great that its free boundary is

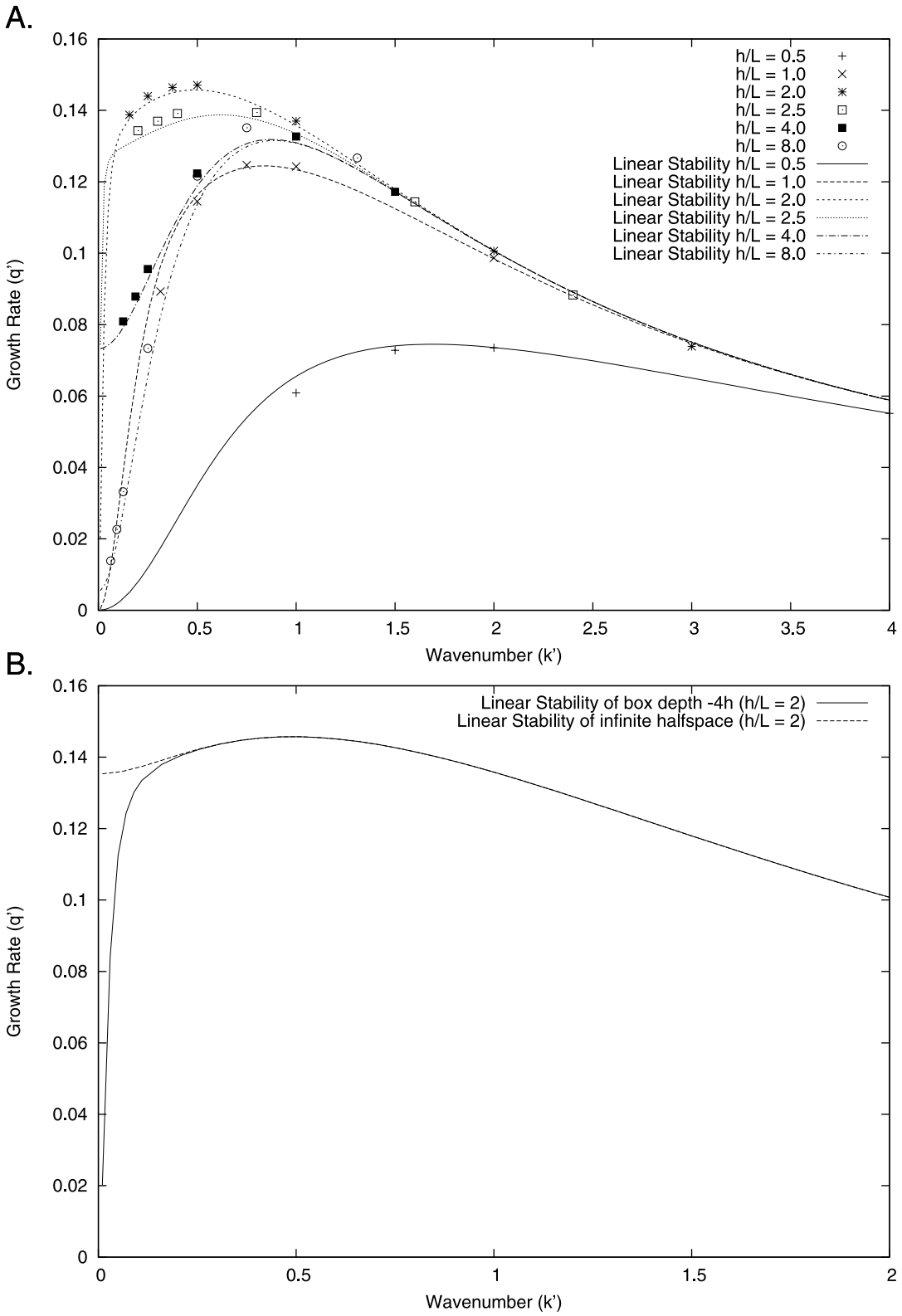

Figure 6. (a) Growth rate factor versus wave number for an experiment with a free top and a viscous substratum from $0 < z < -4h$. Both linear stability (lines) and numerical (points) results shown. (b) Growth rate factor versus wave number as above for case of $h/L = 2$ to show the differences resulting from a substratum extending to a depth of $-4h$ depth approximation as opposed to using an infinite half-space.

essentially removed from the problem. When the ratio of h/L drops below ≈ 8, however, the growth rates transition to a style characteristic of a free top, with finite q' at $k' = 0$. Here, the entire layer is involved in the foundering, and the stress free boundary condition at the surface becomes important.

3.2. Viscous Substratum and Constant Density

[19] We also perform experiments using a viscous substratum, by continuing the exponential viscosity scaling to greater depth. When a viscous substratum is added, in this case to depth of $z = -4h$, the form of the growth rate changes slightly (Figure 6a). For large viscosity variations ($h/L > 8$), growth rate curves again approach those of a calculation of exponential viscosity in two infinite half-spaces, with $q' \rightarrow 0$ as $k' \rightarrow 0$. When the ratio of h/L drops below ≈ 8, however, the growth rates appear to be a blend of both the stress free and fixed-top styles as in Figure 5, showing characteristics of both. For all ratios of $h/L < 8$ examined, $q'_{\max}$ does not occur at a wave number smaller than $k' \approx 0.5$. Yet for several cases, in the $\lim_{k' \rightarrow 0}$, q' remains finite. This contrasts with the behavior for an inviscid substratum in Figure 5, where, for $h/L = 1$ and 2, $q'_{\max}$ occurred at $k' = 0$. Additionally, in Figure 4 we saw the relation

$$\lim_{k' \rightarrow 0} q' \neq 0 \tag{10}$$

applied only when the viscosity of the substratum is zero. Now we observe a range of viscosity scalings that meet this condition. Thus, exponential viscosity introduces a relative enhancement of growth rate at long wavelength (small wave number). Alternatively, the viscous substratum retards the growth rate overall, with increasing effect as $|k'_{q'} \max - k'|$ increases. It also affects the wave number of maximum growth rate, for $k'_{q'}$ max varies with h/L, and reaches a minimum for the value $h/L \approx 2$, not as $h/L \rightarrow 0$.

[20] For both numerical and analytical results, we extend our substratum to a depth of $-4h$. To show the effect of a finite depth on the dependence of q' on k' we plot (Figure 6b) the linear stability curves for both a case with substratum depth limited to $-4h$ (as in Figure 6a) and the same case with an infinite half-space substrate to illustrate the differences resulting from this approximation. The divergence between the growth rates for the two structures is limited to small wave numbers ($k' < 0.25$) and h/L ratios below 4.

[21] As h/L transitions through the intermediate window between the small h/L, stress free and large h/L, fixed-top end-member styles, a plot of $\lim_{k' \rightarrow 0} q'$ with the $\log(h/L)$ for both the viscous (Figure 6) and inviscid substrata (Figure 5) displays a smooth transition (Figures 7a and 7b). We show this plot for two nondimensionalizations; Figure 7a displays dimensionless results with respect to L, and Figure 7b shows them with respect to h. Overall, the difference between the inviscid and viscous cases can be thought of as a result of retardation caused by the viscous substratum. This retarding is concentrated where $h/L < 2$. Both curves (for both scalings) are similar for the region $h/L \gg 1$ as the substratum has little effect due to its relatively low viscosity. In Figure 7a, for values of h/L around 1, we can see that the viscous substratum narrows the band of intermediate growth rate curves, and shifts the peak to a slightly higher h/L value. In Figure 7b, we see that the substratum affects approximately the same h/L range, but with obviously different results. When $h/L \ll 1$, the growth rate factor scaled by h levels to a value of 0.25 as the viscosity variation approximates a constant value.

[22] For small values of h/L ($h/L < 1$), a nondimensionalization using h instead of L becomes more sensible, because the growth of perturbations is driven by the density contrast in the layer of thickness h. In such a case (not shown), $q'(k')$ transforms to the solution for constant viscosity, and again, $\lim_{k' \rightarrow 0}$, q' is zero as in Figure 4.

[23] To understand the long-wavelength enhancement of growth rate, we calculate eigenfunctions for the z component of velocity, w'. Calculating the eigenfunction at infinite wavelength ($k' = 0$) is impossible because the matrix created from applying boundary conditions to the assumed solution form, equation (6), collapses to a determinant of zero regardless of growth rate factor; therefore we show a series of eigenfunctions for a fixed value of $k' = 0.1$ and various values of h/L in Figure 8. With this series we examine the depth distribution of flow at long wavelength. The unstable layer is from $0 < z' < 1$ and the eigenfunction amplitudes have been normalized so that $w'(0) = 1$. When $h/L = 10$, the eigenfunction in the lower layer is highly oscillatory about zero, indicating that material is being turned over in several small-scale sections. For intermediate h/L values, such as $h/L = 1$, the wavelength of the oscillation increases, so that near the layer interface there exists substantial vertical motion. In fact, the curve for $h/L = 10$, the only solution outside the free-top fixed-top transition zone, is the only curve that does not share the same amplitude in the $1 > z' > -1$ region.

[24] Our choice of exponential viscosity in the substrate is one of simplicity. We can compare these growth rate factors to those of the more probable case with constant viscosity in the substrate ($z' < 0$) for several values of h/L (see Figure 9). Aside from the general differences in growth rate factor amplitude, we see only subtle changes in the small k' regions. A constant viscosity substrate alters growth at very long wavelengths ($k' < 0.4$) so that q' approaches zero at $k' = 0$.

3.3. Inviscid Substratum and Linear Varying Density

[25] We also perform experiments with density varying linearly with depth in the layer, shown in Figure 10, for which explicit linear stability solutions cannot be obtained analytically. For a fixed top, linear density has been previously shown to decrease growth rates by $\approx$25% (but strongly dependent on h/L) and to shift the maximum growth rate factor to slightly higher wave numbers [*Conrad and Molnar*, 1997; *Houseman and Molnar*, 1997; *Molnar et al.*, 1998]. We examine whether these same effects of linear density apply under a shear stress free upper boundary condition.

[26] The most striking difference between the cases of linear density and constant density is the smaller growth rate

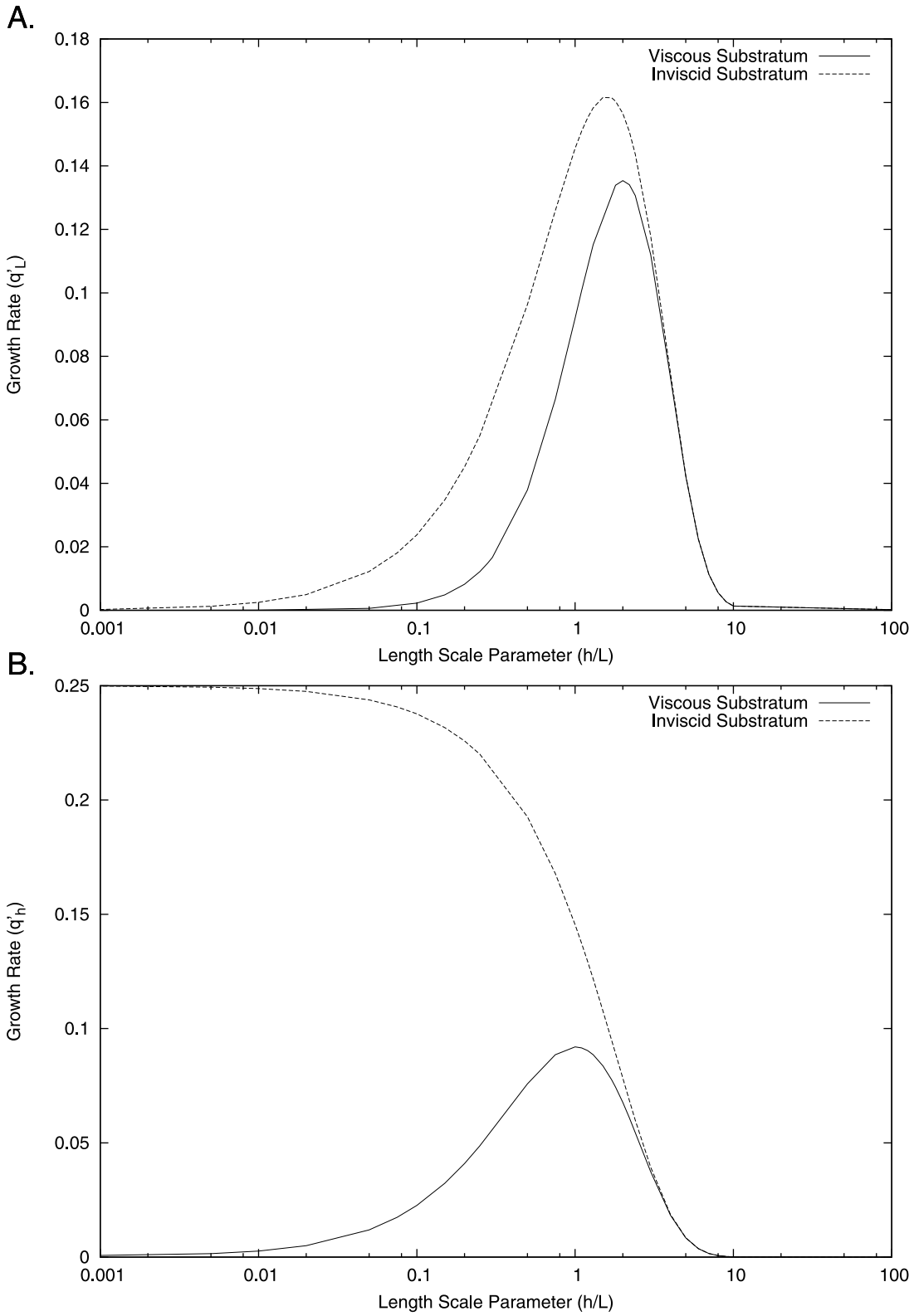

Figure 7. Semilog plots of $\lim_{k'} \to 0\ q'$ versus h/L for substrate continuing to negative infinity. (a) Plot of q' and k' nondimensionalized by L, for both viscous and inviscid stress free top experiments. Here, $q'_L = q\frac{\eta}{\Delta\rho g L}$. (b) Same as Figure 7a but q' and k' nondimensionalized by h, so $q'_h = q\frac{\eta}{\Delta\rho g h}$.

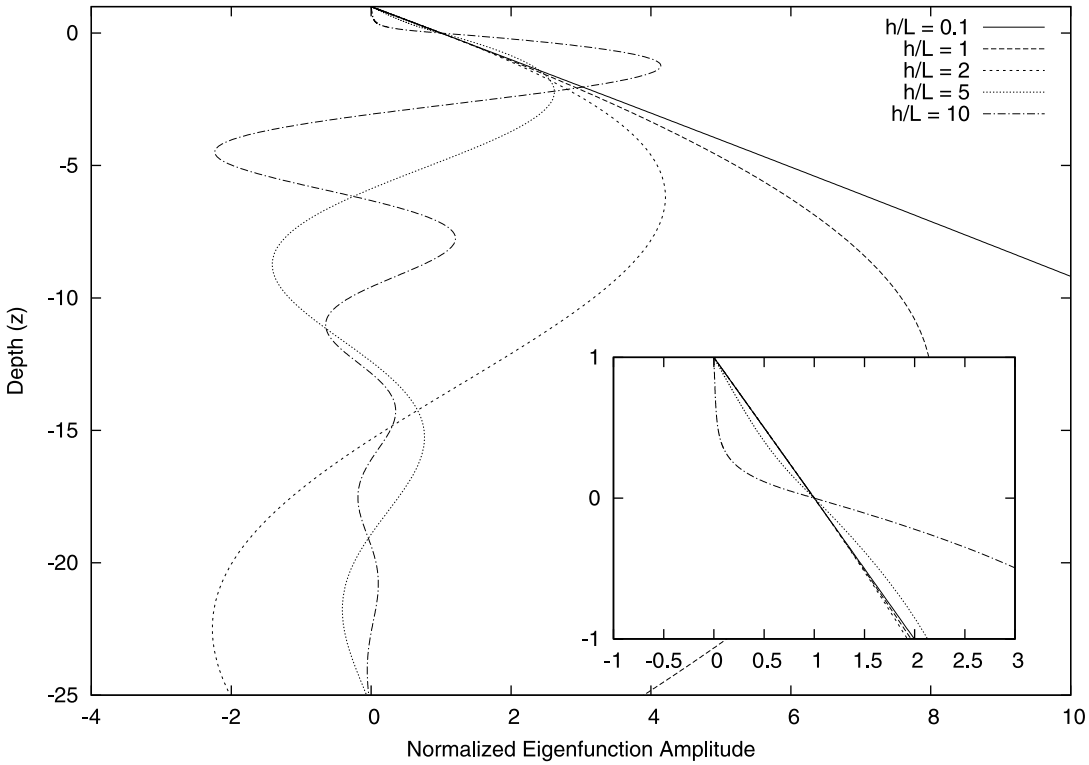

Figure 8. Plots of the downward velocity (w') eigenfunction for a fixed values of $k' = 0.1$ and various values of viscosity scaling, h/L. Experiments are for a layer of thickness 1 with bottom boundary at depth 0. The functions are normalized so that the amplitude is 1 at depth 0. Inset is zoom of area around $z = 0$.

factors for linear density. Comparing these graphs, we observe that $q'_{\max}$ for the curve $h/L = 1$ is ≈35% of its constant density value. The other $q'_{\max}$ values are ≈67% of that for constant density for $h/L = 2$ and ≈80% for $h/L = 4$ and 8. So, the impact of linear density is much greater when viscosity variation in the layer is low ($h/L < 2$).

[27] Comparing the curves for $h/L = 4$ and 8 in both experiments (Figures 5 and 10) also shows that linear density shifts the location of $q'_{\max}$ to lower wave number (longer wavelength). The exact shift (defined as $\Delta k' = (k'_{\max\ \textit{linear density}} - k'_{\max\ \textit{constant density}})/k'_{\max\ \textit{constant density}}$) cannot be found without running calculations at additional k' values, but we estimate $\Delta k' \approx -25\%$. This differs from previous work for a rigid top, as linear density was found to push peak growth rate to higher wave number [*Conrad and Molnar*, 1997; *Molnar et al.*, 1998].

[28] Finally, we notice that for $h/L = 4$, growth rate factors at the longest wavelengths are actually enhanced over their constant density values. Moreover, there is no indication that $q'_{\max} \rightarrow 0$ as $k' \rightarrow 0$.

3.4. Viscous Substratum and Linear Varying Density

[29] Figure 11 shows our results for linear density calculations with a viscous substratum, and displays the three main effects described for the inviscid calculations. Compared to constant density, growth rates are reduced overall, with the greatest effect at small h/L values. For $h/L = 8$, $q'_{\max}$ is ≈85% of the constant density value, and for $h/L = 1$, $q'_{\max}$ is ≈38% of the constant density value. Second, the location of $q'_{\max}$ is shifted to smaller wave number by $\Delta k'$ ≈ 25%. Finally, the growth rate curves for $h/L = 4$ and 2.5 both show some enhancement at long wavelength. $h/L = 4$ has larger absolute growth rates, and the $h/L = 2.5$ curve shows some flattening at long wavelength.

[30] In these calculations, the viscous substratum exerts the same enhancement of q' at low k' compared with fixed top as for constant density. Although we cannot obtain solutions for linear stability, the numerical results suggest that in the $\lim_{k' \rightarrow 0}$, q' will be finite, for a $2 < h/L < 4$.

4. Non-Newtonian Exponentially Varying Viscosity With Depth

[31] We perform additional numerical calculations of a layer over an inviscid half-space using a nonlinear viscosity exponent, $n = 3$, in the constitutive equation, equation (2). Again, our interest is examining how nonlinear viscosity interacts with a shear stress free top boundary to affect the growth rate of the downwelling. We again carried out two sets of experiments, one with constant density in the layer, and another with linearly varying density. As before, each set is performed for various wave numbers and viscosity scalings. Unfortunately, the nonlinear viscosity exponent means that for a scaling of $h/L = 4$ the effective variation of

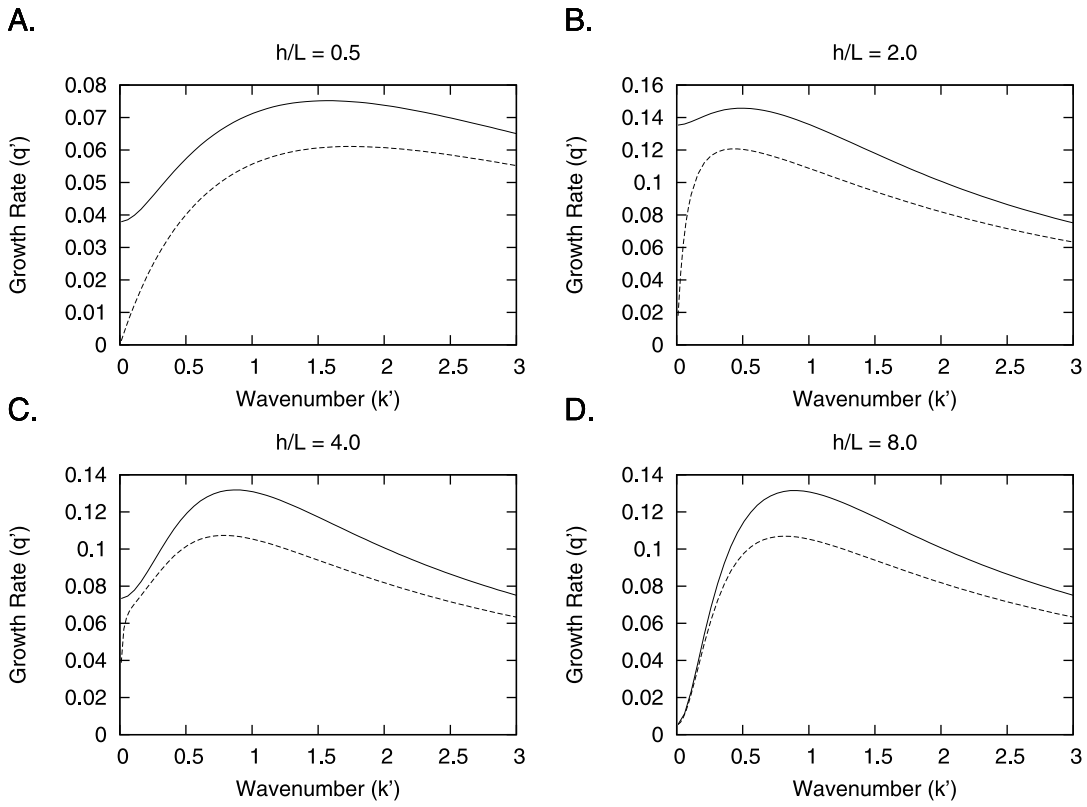

Figure 9. Growth rate factor versus wave number from linear stability cases with infinite depth for various *h/L* values. Solid curves are previous data (Figure 6a) from experiments with exponential viscosity in the substratum. Dashed curves are for constant viscosity in the substratum. For (a) $h/L = 0.5$, (b) $h/L = 2.0$, (c) $h/L = 4.0$, and (d) $h/L = 8.0$.

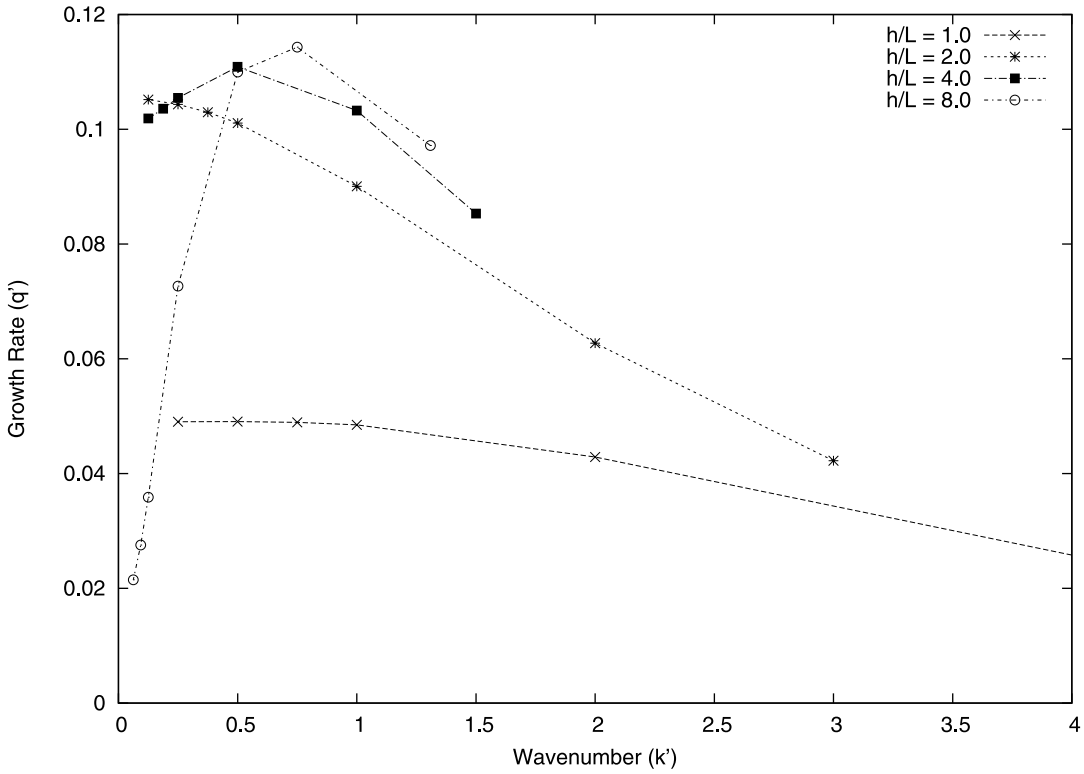

Figure 10. Growth rate versus wave number for various values of *h/L*. Numerical results are shown for experiments with linear varying density, exponential viscosity varying with depth, and a free top boundary condition. These calculations also assume an inviscid constant density substratum.

viscosity in the layer becomes $(e^4)^3$. This large variation prevented us from examining larger values of *h/L*.

[32] Our results for linearly varying density with an inviscid substrate are seen in Figure 12. Overall, this calculation exhibits some of the same characteristics of similar calculations with Newtonian viscosity (Figure 10). At large wave numbers ($k' > 2$), growth rates increase monotonically as viscosity variation in the layer increases. These calculations also have smaller (≈50%) growth rate factors than their constant density counterparts (not shown), as expected. They also share the finding that q' is finite as $k' \rightarrow 0$. What is surprising in these results is that for the for case $h/L = 4$ in Figure 12, a local minimum of growth rate factor develops at $k' \approx 0.25$. Further work examining this behavior is forthcoming.

5. Discussion/Conclusions

[33] The Rayleigh-Taylor calculations show that the overall effect of a shear stress free top boundary condition is to enhance growth rates at long wavelengths, $k' < 0.5$ ($\lambda > 4\pi L$). The degree of enhancement depends also, however, on exponential viscosity variation, linear density variation, and/or the presence of a viscous substratum.

[34] Linearly decreasing density reduces growth rates relative to those for constant density in the layer, as expected. Interestingly, however, linearly decreasing density also enhances long-wavelength growth rates for a narrow band of viscosity depth profiles. Specifically, we noticed that when $h/L = 4$, long wavelengths grow faster for linear density than for constant density (Figure 11). Considering these rheological scalings together, we have retardation that leaves wave numbers near $k' \approx 0.5$ minimally affected, little decrease in q' at $0.2 < k' < 0.5$, and the shifting of $k'_{q'\max}$ toward long wavelengths ($k' \approx 0.5$) as in Figure 11, compared to fixed top calculations.

[35] Differences between the free and fixed-top cases vary with *h/L* and disappear when $h/L > 8$. For instance, for $h/L \approx 2.5$, $q'_{\max}$ occurs at wave numbers of $k'_{free} \approx 0.3$ (Figure 11) and $k'_{fixed} \approx 1.2$ [*Molnar et al.*, 1998, Figure 7] for free and fixed tops, respectively. When $h/L \approx 4$ the difference decreases so that $q'_{\max}$ occurs at wave numbers of $k'_{free} \approx 0.6$ and $k'_{fixed} \approx 0.8$. With a free top, since several growth rate curves flatten for small k' values, but those for the fixed top do not, $q'_{\max}$ is less important as it is where q' decreases rapidly with decreasing k', and greater differences between fixed and free tops seem permissible [*Molnar et al.*, 1998].

[36] The implications for the deformation of the mantle lithosphere can be seen in comparison to the Sierra Nevada in California. Two high seismic wave speed anomalies in the mantle underlie the Sierra Nevada. If the two anomalies formed by similar Rayleigh-Taylor processes, they would define a natural wavelength for this mechanism. Before we apply the scaling relations presented above to the Sierra Nevada, let us note that they do not offer unique explan-

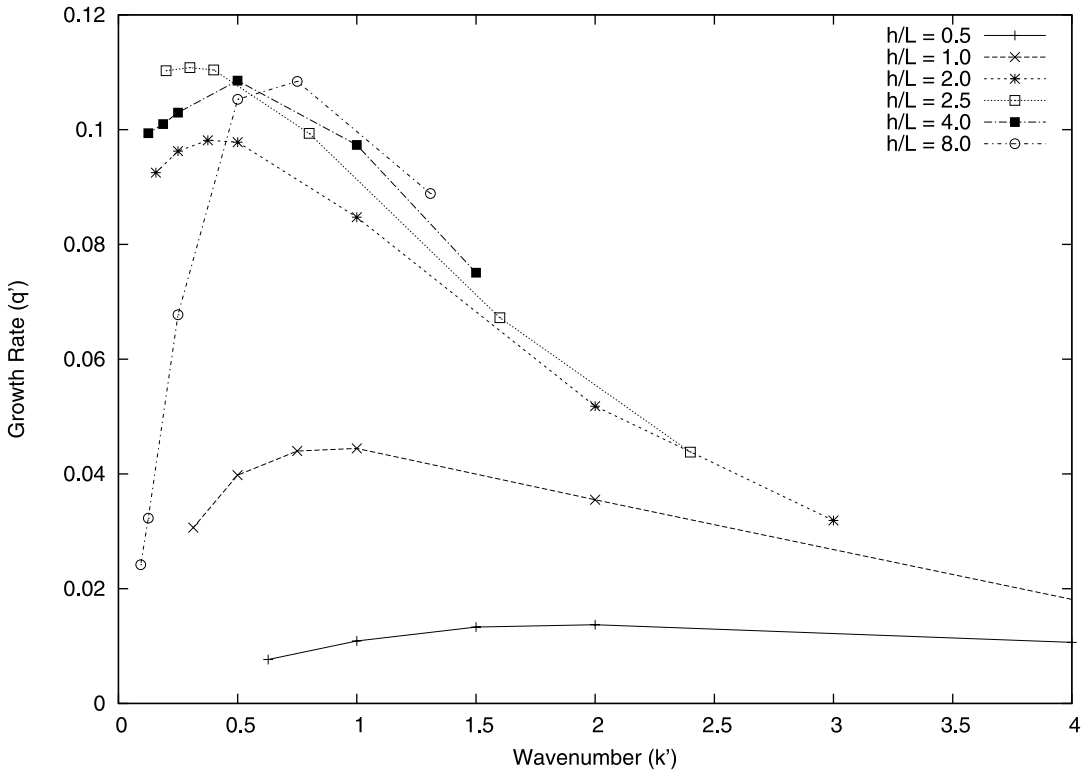

Figure 11. Growth rate versus wave number for various values of *h/L*. Numerical results are shown for experiments with linear varying density, exponential viscosity varying with depth, and a free top boundary condition. These results also have a viscous substratum.

ations for the long distance between the Redding and Isabella anomalies, which we presume to mark zones of downwelling in the upper mantle. First, we apply relationships derived for two-dimensional flow to a three-dimensional structure. The locations of the two anomalies at the northern and southern ends of the Sierra Nevada, which itself shows marked east–west variations, implies that the third, east–west dimension could be important. Second, we have assumed that the material is isotropic. Recent work by *Lev and Hager* [2008] shows that anisotropy can affect the wavelength of maximum growth. In particular, resistance to shear on horizontal (or vertical) planes was much less than that on planes dipping at 45°, and the maximum growth rate could increase two to perhaps three times.

[37] As noted, the dimensional wavelength from calculations depends on the choice of *h/L*, and we should consider the realistic scaling ratio, *h/L*, of the Sierra Nevada mantle lithosphere. Using a linear geotherm in the lithosphere,

$$T(z) = T_0 - \beta z \tag{11}$$

(remembering $z = 0$ at the base of the lithosphere) the viscosity can be expressed from olivine laboratory experiments [*Kohlstedt et al.*, 1995] as approximately

$$\eta = \left[\frac{1}{2}A^{-1/n}(\epsilon_{xx})^{1-n/n}\exp\left(\frac{E_a}{nRT_0}\right)\right]\exp(\gamma z) \tag{12}$$

where A is constant and [*Conrad and Molnar*, 1997]

$$\gamma = \frac{E_a\beta}{nRT_0^2} = \frac{E_a}{nRT_0^2}\frac{\Delta T}{h} = \frac{1}{L}$$
$$\therefore\ \frac{h}{L} = \frac{E_a\Delta T}{nRT_0^2} \tag{13}$$

Parameter descriptions are given in the notation section.

[38] Using reasonable values of activation energy E_a between 400 and 600 kJ/mol K, temperature $1000 < T_0 < 1600$°K ($727 < T_0 < 1327$°C), $370 < \Delta T < 1130$°K, and stress-strain exponent n as 3.5, the ratio *h/L* for the Sierra Nevada varies from 5 to 9. This places the Sierra Nevada scaling ratio at the upper limit of the range of *h/L* values from our experiments [*Conrad and Molnar*, 1997; *Kohlstedt et al.*, 1995; *Lachenbruch and Sass*, 1977; *Saltus and Lachenbruch*, 1991].

[39] For example, for $h/L = 6$, and a combined eclogite layer and mantle lithosphere thickness (h) of 200 km, would yield a $L \approx 33$ km. We remind the reader that although our experiments are 2-D plain strain calculations, the Sierra Nevada deformation is certainly 3-D, and the effective k' would be a combination of the wave numbers of disturbances parallel and perpendicular to the range (i.e., $k'_{eff} = \sqrt{k'^2_{\parallel} + k'^2_{\perp}}$) [*Kerr and Lister*, 1988]. Thus we can consider as a minimum the Sierra Nevada range parallel natural wavelength, which is approximately 500km. Setting wavelength as $2\pi L/k' = 500$ km implies $k' \approx 0.4$. As noted above,

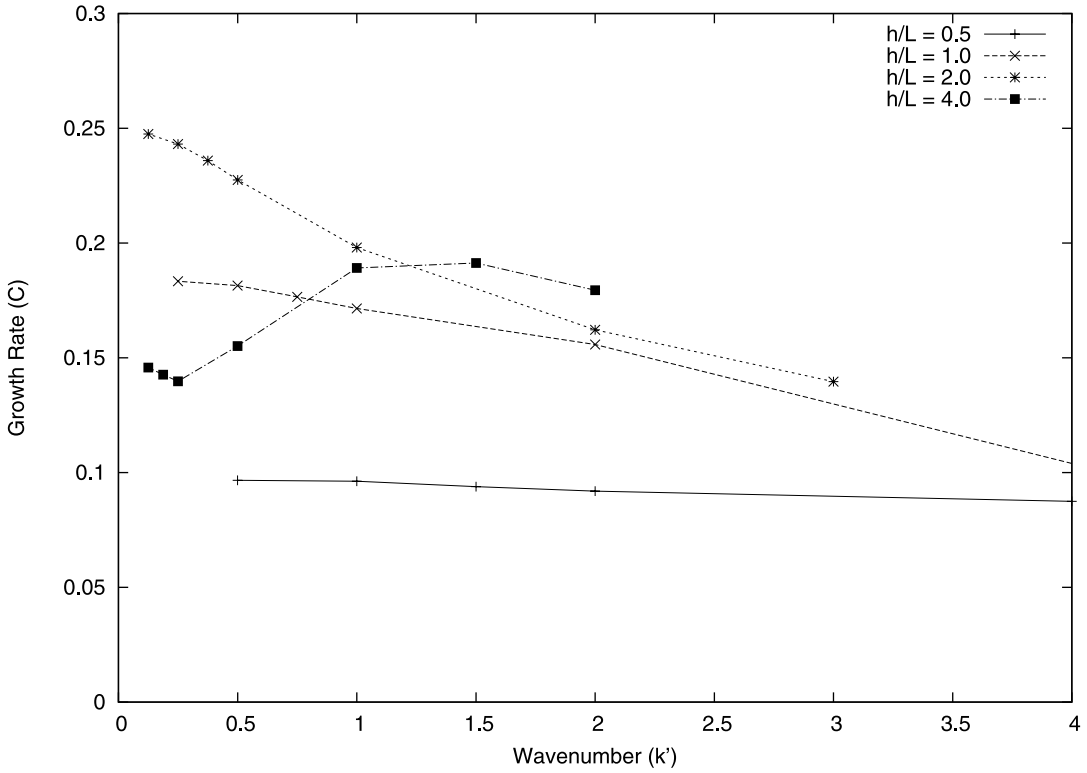

Figure 12. Growth Rate versus wave number for cases with nonlinear viscosity ($n = 3$) with several h/L viscosity scalings. These calculations have linearly varying density and an inviscid substrate.

this rapid growth of instability with such a λ seems more permissible with a free top, because the growth rate factors decrease little for $k' < 0.5$. Thus when viscosity decreases with depth and the top surface of the unstable layer is only weakly constrained longer wavelengths than commonly assumed for Rayleigh-Taylor instabilities should be considered.

Notation

- B viscosity coefficient (where constant in the layer).
- B_0 viscosity coefficient at the base of the layer, through which it decreases with depth.
- β geothermal temperature gradient.
- $\dot{E}$ second invariant of the strain rate tensor.
- E_a activation energy.
- g gravitational acceleration.
- h thickness of layer.
- k wave number of perturbation to the base of the layer.
- $\Delta k'$ shift in $k'_{\max}$ seen in experiments with linearly varying density.
- L characteristic e-folding depth scale for exponential decrease in viscosity coefficient.
- p pressure.
- q growth rate of Rayleigh-Taylor instability for Newtonian viscosity.
- R gas law constant.
- t time.
- T temperature.
- T_0 temperature at base of layer.
- ΔT temperature difference across layer.
- u horizontal component of velocity.
- w vertical component of velocity.
- x horizontal coordinate.
- z vertical coordinate.
- $\Delta\rho$ density difference between the layer and the underlying half-space or subspace.
- σ_{ij} stress component.
- τ_{ij} deviatoric stress component.

[40] **Acknowledgments.** This research was supported by the National Science Foundation grant EAR-0607831. We thank C. Jones and H. Reeg for providing Sierra Nevada tomography results for Figure 1 and W. Szeliga for helpful discussions. This work benefited from constructive criticisms from two anonymous reviewers.

References

Atwater, T., and J. Stock (1998), Pacific-North America plate tectonics of the Neogene southwestern United States: An update, *Int. Geol. Rev.*, *40*, 375–402.

Austrheim, H. (1991), Eclogite formation and dynamics of crustal roots under continental collision zones, *Terra Nova*, *3*, 492–499.

Benz, H. M., and G. Zandt (1993), Teleseismic tomography: Lithospheric structure of the San Andreas fault system in northern and central California, in

Seismic Tomography: Theory and Practice, edited by H. M. Iyer and K. Hirahara, pp. 440–465, Chapman and Hall, London.

Bird, P. (1978), Initiation of intracontinental subduction in the Himalaya, *J. Geophys. Res.*, *83*, 4975–4987.

Brace, W. F., and D. L. Kohlstedt (1980), Limits on lithospheric stress imposed by laboratory experiments, *J. Geophys. Res.*, *85*, 6248–6252.

Canright, D., and S. Morris (1993), Buoyant instability of a viscous film over a passive fluid, *J. Fluid Mech.*, *255*, 349–372.

Chandrasekhar, S. (1961), *Hydrodynamic and Hydromagnetic Stability*, Oxford Univ. Press, Oxford, U.K.

Conrad, C. P., and P. Molnar (1997), The growth of Rayleigh-Taylor-type instabilities in the lithosphere for various rheological and density structures, *Geophys. J. Int.*, *129*, 95–112.

Dewey, J. F., and J. M. Bird (1970), Mountain belts and the new global tectonics, *J. Geophys. Res.*, *75*, 2625–2647.

Dewey, J. F., and K. C. A. Burke (1973), Tibetan, Variscan, and Precambrian basement reactivation: Products of continental collision, *J. Geol.*, *81*, 683–692.

Dricker, I. G., and S. W. Roecker (2002), Lateral heterogeneity in the upper mantle beneath the Tibetan plateau and its surroundings from SS-S travel time residuals, *J. Geophys. Res.*, *107*(B11), 2305, doi:10.1029/2001JB000797.

Ducea, M. N., and J. B. Saleeby (1996), Bouyancy sources for a large, unrooted mountain range, the Sierra Nevada, California: Evidence from xenolith thermobarometry, *J. Geophys. Res.*, *101*(B4), 8229–8244.

Ducea, M. N., and J. B. Saleeby (1998), A case for delamination of the deep batholithic crust beneath the Sierra Nevada, California, *Int. Geol. Rev.*, *133*, 78–93.

England, P., and G. Houseman (1989), Extension during continental convergence, with application to the Tibetan Plateau, *J. Geophys. Res.*, *94*, 17,561–17,579.

Farmer, G. L., A. F. Glazner, and C. R. Manley (2002), Did lithospheric delamination trigger late Cenozoic potassic volcanism in the southern Sierra Nevada, California?, *Geol. Soc. Am. Bull.*, *114*, 754–768.

Fletcher, R. C., and B. Hallet (1983), Unstable extension of the lithosphere: A mechanical model for Basin-and-Range structure, *J. Geophys. Res.*, *88*, 7457–7466.

Fountain, D. M., and N. I. Christensen (1989), Composition of the continental crust and upper mantle: A review, in *Geophysical Framework of the Continental United States*, edited by L. C. Pakiser and W. D. Mooney, *Mem. Geol. Soc. Am.*, *179*, 711–742.

Hartog, R., and S. Y. Schwartz (2000), Subduction-induced strain in the upper mantle east of the Mendocino triple junction, California, *J. Geophys. Res.*, *105*, 7909–7930.

Hoogenboom, T., and G. A. Houseman (2006), Rayleigh-Taylor instability as a mechanism for corona formation on Venus, *Icarus*, *180*, 292–307.

Houseman, G. A., and P. Molnar (1997), Gravitational (Rayleigh-Taylor) instability of a layer with nonlinear viscosity and convective thinning of continental lithosphere, *Geophys. J. Int.*, *128*, 125–150.

Houseman, G. A., D. P. McKenzie, and P. Molnar (1981), Convective instability of a thickened boundary layer and its relevance for the thermal evolution of continental convergent belts, *J. Geophys. Res.*, *86*, 6115–6132.

Jones, C. H., and R. A. Phinney (1999), Prospecting for the petrology of the upper mantle: Teleseismic shear waves in the Sierra Nevada, California, *Geol. Soc. Am. Abstr. Programs*, *31*(7), A481.

Jones, C. H., H. Kanamori, and S. W. Roecker (1994), Missing roots and mantle "drips": Regional Pn and teleseismic arrival times in the southern Sierra Nevada and vicinity, California, *J. Geophys. Res.*, *99*, 4567–4601.

Jones, C. H., G. L. Farmer, and J. Unruh (2004), Tectonics of Pliocene removal of the lithosphere of the Sierra Nevada, California, *Geol. Soc. Am. Bull.*, *116*, 1408–1422.

Jull, M., and P. B. Keleman (2001), On the conditions for lower crustal convective instability, *J. Geophys. Res.*, *106*, 6423–6446.

Kerr, R. C., and J. R. Lister (1988), Island arc and mid-ocean ridge volcanism, modelled by diapirism from linear source regions, *Earth Planet. Sci. Lett.*, *88*, 143–152.

Kohlstedt, D. L., B. Evans, and S. J. Mackwell (1995), Strength of the lithosphere: Constraints imposed by laboratory experiments, *J. Geophys. Res.*, *100*, 17,587–17,602.

Lachenbruch, A. H., and J. H. Sass (1977), Heat flow in the United States and the thermal regime of the crust, in *The Earth's Crust: Its Nature and Physical Properties*, *Geophys. Monogr. Ser.*, vol. 20, edited by J. G. Heacock, pp. 626–675, AGU, Washington, D. C.

Le Pourhiet, L., M. Gurnis, and J. Saleeby (2006), Mantle instability beneath the Sierra Nevada Mountains in California and Death Valley extension, *Earth Planet. Sci. Lett.*, *251*, 104–119.

Lee, C.-T., R. L. Rudnick, and G. H. Brimhall, Jr. (2001), Deep lithospheric dynamics beneath the Sierra Nevada during the Mesozoic and Cenozoic as inferred from xenolith petrology, *Geochem. Geophys. Geosyst.*, *2*(12), 1053, doi:10.1029/2001GC000152.

Lev, E., and B. H. Hager (2008), Rayleigh - Taylor instabilities with anisotropic lithospheric viscosity, *Geophys. J. Int.*, *173*(3), 806–814.

McNamara, D. E., W. R. Walter, T. J. Owens, and C. J. Ammon (1997), Upper mantle velocity structure beneath the Tibetan Plateau from Pn travel time tomography, *J. Geophys. Res.*, *102*, 493–505.

Molnar, P. (1990), S-wave residuals from earthquakes in the Tibetan region and lateral variations in the upper mantle, *Earth Planet. Sci. Lett.*, *101*, 68–77.

Molnar, P., and C. H. Jones (2004), A test of laboratory based rheological parameters of olivine from an analysis of late Cenozoic convective removal of mantle lithosphere beneath the Sierra Nevada, California, USA, *Geophys. J. Int.*, *156*, 555–564.

Molnar, P., G. A. Houseman, and C. P. Conrad (1998), Rayleigh-Taylor instability and convective thinning of mechanically thickened lithosphere: Effects of non-linear viscosity decreasing exponentially with depth and of horizontal shortening of the layer, *Geophys. J. Int.*, *133*, 568–584.

Moresi, L.-N., and V. S. Solomatov (1995), Numerical investigation of 2D convection with extremely large viscosity variations, *Phys. Fluids*, *7*(9), 2154–2162.

Neil, E. A., and G. A. Houseman (1999), Rayleigh-Taylor instability of the upper mantle and its role in intraplate orogeny, *Geophys. J. Int.*, *138*, 89–107.

Ni, J., and M. Barazangi (1983), High-frequency seismic wave propagation beneath the Indian Shield, Himalayan Arc, Tibetan Plateau and surrounding regions: high uppermost mantle velocities and efficient S_n propagation beneath Tibet, *Geophys. J.R. Astron. Soc.*, *72*, 665–689.

Owens, T. J., and G. Zandt (1997), Implications of crustal property variations for models of Tibetan plateau evolution, *Nature*, *387*, 37–43.

Özalaybey, S., and M. K. Savage (1995), Shear wave splitting beneath western United States in relation to plate tectonics, *J. Geophys. Res.*, *100*, 18,135–18,149.

Reeg, H., C. H. Jones, H. Gilbert, T. Owens, and G. Zandt (2007), Teleseismic travel-time tomography of the Sierra Nevada and its foundering lithosphere, *Eos Trans. AGU*, *88*(52), Fall Meet. Suppl., Abstract T33A-1150.

Saleeby, J., and Z. Foster (2004), Topographic response to mantle lithosphere removal in the southern Sierra Nevada region, California, *Geology*, *32(3), 245–248.*

Saltus, R. W., and A. H. Lachenbruch (1991), Thermal evolution of the Sierra Nevada: Tectonic implications of new heat flow data, *Tectonics*, *10*, 325–344.

Sibson, R. H. (1977), Fault rocks and fault mechanisms, *J. Geol. Soc., London*, *133*, 191–213.

Sibson, R. H. (1982), Fault zone models, heat flow, and the depth distribution of earthquakes in the continental crust of the United States, *Bull. Seismol. Soc. Am.*, *72*, 151–163.

Stock, G. M., R. S. Anderson, and R. C. Finkel (2004), Pace of landscape evolution in the Sierra Nevada, California, revealed by cosmogenic dating of cave sediments, *Geology*, *32*, 193–196.

Tilmann, F., J. Ni, and INDEPTH III Seismic Team (2003), Seismic imaging of the downwelling Indian lithosphere beneath central Tibet, *Science*, *300*, 1424–1427.

Unruh, J. R. (1991), The uplift of the Sierra Nevada and implications for late Cenozoic epeirogeny in the western Cordillera, *Geol. Soc. Am. Bull.*, *103*, 1395–1404.

Whitehead, J. A., and D. S. Luther (1975), Dynamics of laboratory diapir and plume models, *J. Geophys. Res.*, *92*, 4817–4825.

Willett, S. D., and C. Beaumont (1994), Subduction of Asian lithospheric mantle beneath Tibet inferred from models of continental collision, *Nature*, *369*, 642–645.

Woodward, R. L., and P. Molnar (1995), Lateral heterogeneity in the upper mantle and SS-S traveltime intervals for SS rays reflected from the Tibetan Plateau and its surroundings, *Earth Planet. Sci. Lett.*, *135*, 139–148.

Zhao, W.-L., and W. J. Morgan (1985), Uplift of Tibetan Plateau, *Tectonics*, *4*, 359–369.

C. Harig and P. Molnar, Department of Geological Sciences, CIRES, University of Colorado, Benson Earth Sciences Building, Boulder, CO 80309, USA. (harig@colorado.edu; molnar@colorado.edu)

G. A. Houseman, Institute of Geophysics and Tectonics School of Earth and Environment, University of Leeds, Leeds LS2 9JT, UK. (greg@earth.leeds.ac.uk)